

Contents lists available at [ScienceDirect](https://www.sciencedirect.com)

Optik

journal homepage: [www.elsevier.com/locate/ijleo](http://www.elsevier.com/locate/ijleo)

# Third-order nonlinear optical effects of silver nanoparticles and third harmonic generation from their plasma plumes

Srinivasa Rao Konda<sup>a,\*</sup>, Sandeep Kumar Maurya<sup>a</sup>, Rashid A. Ganeev<sup>a,c</sup>,  
Yu Hang Lai<sup>a</sup>, Chunlei Guo<sup>b,\*</sup>, Wei Li<sup>a,\*</sup>

<sup>a</sup> GPL, State Key Laboratory of Applied Optics, Changchun Institute of Optics, Fine Mechanics and Physics, Chinese Academy of Sciences, Changchun 130033, China

<sup>b</sup> The Institute of Optics, University of Rochester, Rochester, NY 14627, USA

<sup>c</sup> University of Latvia, Riga LV-1586, Latvia

## ARTICLE INFO

### Keywords:

Ag nanoparticles  
Third-order nonlinear optical properties  
Plasma plume  
Z-scan measurements

## ABSTRACT

We investigated the third-order nonlinear optical (NLO) properties of the silver (Ag) nanoparticles (NPs) of various sizes, which were produced by disintegration of commercially available 20 and 100 nm NPs in different solvents. It is observed that NPs with the sizes less or greater than 30 nm possess saturable absorption or reverse saturable absorption (or two-photon absorption), respectively. The NPs suspensions show a self-focusing effect. In addition, the third harmonic generation from the plasma plumes produced by nanosecond laser ablation of bulk Ag and Ag NPs of 100 nm and 20 nm sizes is reported. The third harmonic efficiency from the plasmas containing NPs was higher compared with the plasmas produced on the bulk silver. Finally, the ionization probabilities of Ag atom and Ag<sup>+</sup> were calculated.

## 1. Introduction

The research on metal nanoparticles (NPs), quantum dots and nanocrystals is essential because of their potential applications in optics, energy harvesting, communications, defense, and medicine [1–15]. The advantages in applications of NPs are also possible due to the appearance of the surface plasmon resonance (SPR), which is responsible for the enhancement of the third-order optical nonlinearities caused by the reduced dimensionality of those species. Numerous noble metal NPs have been studied under different conditions using various intense laser pulses (for example [16–18]). Among them, Ag NPs possess significant nonlinear optical (NLO) properties [19–26], due to their strong SPR in the visible spectral range [27–30]. A unique property of spherical Ag NPs is that their SPR peak can be tuned between 400 nm and 530 nm by changing the particle size. Even larger shifts of SPR peak towards the infrared region can be achieved by using rod- or plate-shaped NPs [27,28,31]. Recently some research groups explored the advanced NLO properties of Ag NPs coupled with Cu and ZnO NPs as well as other NPs [19–26].

Earlier, Ag NPs have been prepared by laser ablation of bulk Ag target and by chemical reduction methods. As it was mentioned, various applications of Ag NPs are related with their size and shape-dependent properties [32–34]. Our group has recently reported the NLO studies of 8 and 50 nm Ag NPs prepared by laser ablation of bulk Ag in deionized water using nano-, pico- and femtosecond pulses. We have shown that the change in the ablated pulse duration leads to the control of size distribution (SD) of NPs [35]. Additionally, the

\* Corresponding authors.

E-mail addresses: [ksrao@ciomp.ac.cn](mailto:ksrao@ciomp.ac.cn) (S.R. Konda), [chunlei.guo@rochester.edu](mailto:chunlei.guo@rochester.edu) (C. Guo), [weili1@ciomp.ac.cn](mailto:weili1@ciomp.ac.cn) (W. Li).

<https://doi.org/10.1016/j.ijleo.2021.167680>

Received 10 June 2021; Received in revised form 12 July 2021; Accepted 19 July 2021

Available online 21 July 2021

0030-4026/© 2021 Elsevier GmbH. All rights reserved.

size effect of NPs leads to the change of their absorption mechanism, i.e. saturable absorption (SA) and reverse saturable absorption (RSA) [36]. It is known that separated NPs attract great attention because of their physical and chemical properties often deviate from both the corresponding bulk materials and aggregated NPs [19].

Even though several articles demonstrated the third-order NLO properties of Ag NPs of various sizes [32,37,38], a detailed investigation of the dependence of NLO properties on the specific SD of Ag NPs is still of great importance, since the Ag NPs size variations lead to the change of their SPR peaks and nonlinear absorption/refraction mechanisms. Laser irradiation is an effective method to produce isolated NPs from fragmented/aggregated NPs [39]. The SD of NPs depends on the solvent's viscosity and surface energy due to changes in the fluence of laser pulses propagating in the solvents. The SA, two-photon absorption (2PA), optical limiting (OL), and optical Kerr nonlinearities are the mechanisms that are responsible for the NLO properties [40–46]. SA dominates usually in the presence of linear absorption [23] whereas RSA may modify absorption at high peak intensities [44,47,48]. With the depletion of the ground state with the increase of the incident laser energies, the nonlinear medium absorbed a high amount of laser energy via excited-state absorption which leads to RSA. These processes depend not only on the energy of the incident photon but also on the excitation wavelength, which plays an important role depending on the resonant or non-resonant transitions [35,49].

In this paper, the prepared NPs were studied using the Z-scan technique. We show that they will be useful in the field of optics and photonics devices. Also, due to the higher NLO properties of Ag NPs combined with other metallic NPs, they can demonstrate significant applications in optics and biomedicine [1–15]. The plasma plumes of NPs with sizes of 100 nm and 20 nm will be useful for high-order harmonic generation and the next generation of tabletop extreme ultraviolet light sources.

## 2. Experimental methods

### 2.1. Laser irradiation

0.5 mg Ag NPs of 100 nm and 20 nm were separately dissolved in 50 ml of DMSO and toluene. The 6 ns, 50 mJ pulses of fundamental wavelength 1064 nm of Nd:YAG laser system (Q-smart 850) is focused by a spherical lens of 100 mm focal length on the suspension surface (Fig. 1(a)). The suspension is placed on a glass holder and rotated with fixed velocity up to 30 mins and subsequently subjected to UV–visible absorption spectroscopy (Agilent Technologies), Scanning electron microscopy (SEM) [S-4800,

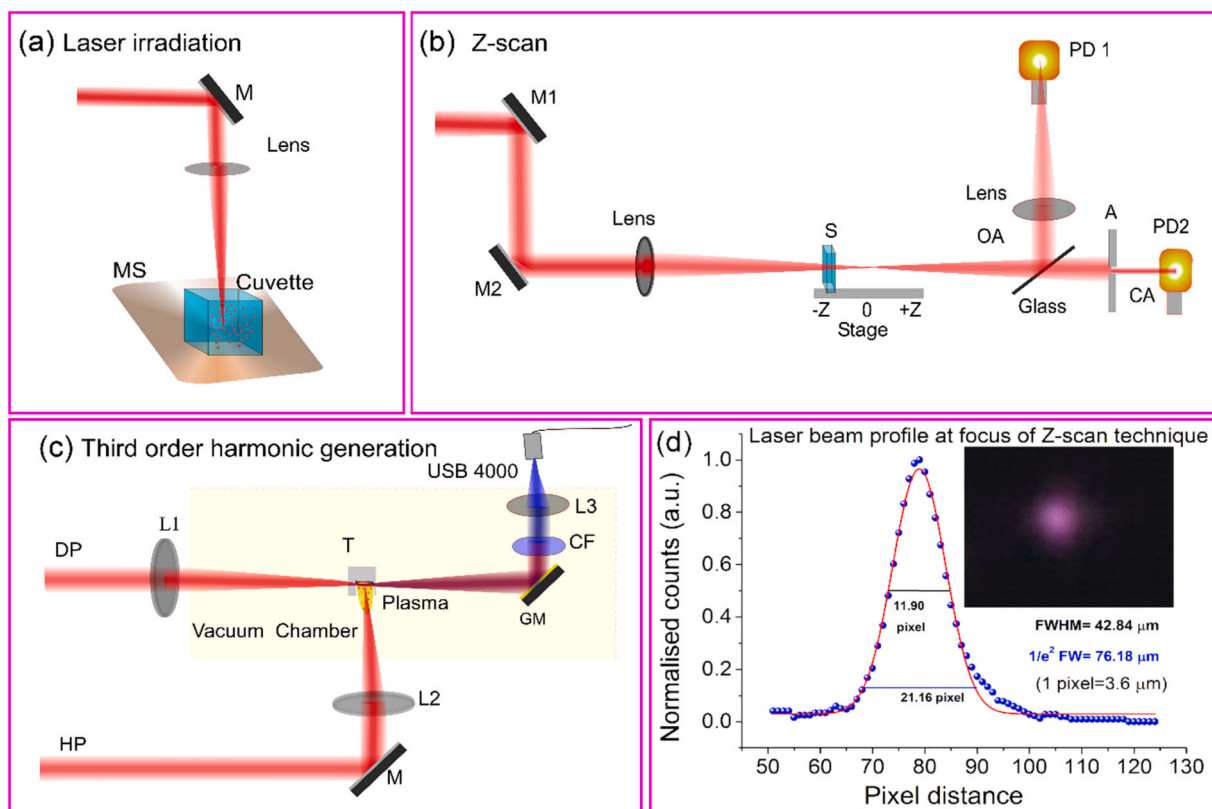


**Fig. 1.** Experimental layouts for a) laser irradiation, MS: magnetic stirrer, lens  $f=100$  mm, M: mirror, b) Z-scan, M1, M2: Mirrors, Lens,  $f=400$  mm, A: Aperture, PD1-photodiode for open aperture (OA), PD2: photodiode for closed aperture (CA). c) THG, DP: driving pulse 800 nm, 35 fs, HP: heating pulse 1064 nm, 6 ns, L1-L3: lens, corresponding focal lengths  $f_1=500$  mm,  $f_2=200$  mm, and  $f_3=500$  mm, respectively, GM: Gold mirror, T: target (Ag bulk, Ag 100 nm and 20 nm nanoparticles). (d) Laser beam profile at the focus of the Z-scan path.

Hitachi], and Z-scan measurements to find the SPR properties, morphology and NLO coefficients respectively.

## 2.2. Z-scan measurements

We used Ti: sapphire (Spectra-Physics, Spitfire Ace) laser pulses (800 nm, 60 fs, 1 kHz) of 0.2  $\mu\text{J}$  with linear (horizontal) polarization [Fig. 1(b)]. The NPs suspension is filled in 1-mm thick cuvette and is scanned along the Z-axis of the focused laser beam ( $f=400$  mm). The Ag NPs nonlinear absorption coefficients and saturation intensities are measured using open aperture (OA) Z-scans. Whereas, the nonlinear refraction coefficients are measured by using closed aperture (CA) Z-scans, where the aperture was narrowed to allow transmitting  $\sim 10\%$  of input radiation. The laser beam profile before keeping the sample is measured at the focus of the Z-scan path using CCD (Thorcam) (Fig. 1(d)) and fitted with Gaussian function and found full width half maximum and  $1/e^2$  beam waist is 42.84 and 76.18  $\mu\text{m}$ , respectively.

## 2.3. THG

The studies used a Ti: Sapphire laser operating at 800 nm, 35 fs, 1 kHz. The 1064 nm, 6 ns used to create the plasma from Ag bulk and NPs (100 nm, 20 nm) in a vacuum chamber. The nanoseconds heating pulses (HP) were focused on the sample surface using a spherical lens of 200 mm focal length ( $1/e^2$  beam radius at focus is: 34.5  $\mu\text{m}$ ). The driving pulse (DP) was focused using a spherical lens of 500 mm focal length ( $1/e^2$  beam radius at focus is: 43.5  $\mu\text{m}$ ) propagating parallel to the sample surface and perpendicular to the propagation axis of HP, as shown in Fig. 1(c). The harmonics yield optimized by adjusting the distance between the target and DP optical axis and the focal position of the HP. The generated third harmonic (TH) radiation from the excited plasma sent out from the target chamber by a gold mirror and the TH signal was separated by the color filter. Then, the spectra of TH radiation is measured using a USB fiber spectrometer (Ocean Optics, USB 4000 +).

## 3. Results and discussion

Section-3.1 deals laser irradiation process and characterization of Ag NPs disintegrated in DMSO, and toluene using UV-visible absorption spectra and SEM analysis. Section 3.2 shows the third-order nonlinearities of the disintegrated NPs of Ag 100 nm and 20 nm using Z-scan measurements. Section 3.3 shows THG from bulk Ag and original (not disintegrated ones) 100 nm, 20 nm NPs for different DP and HP intensities, and ionization probability calculations of Ag atom and  $\text{Ag}^+$  ion.

### 3.1. Characterization of Ag NPs in DMSO and toluene

The commercial 100 nm and 20 nm NPs are aggregated in two solvents (DMSO and Toluene, which have a density of 1.1004, 0.87  $\text{g}/\text{cm}^3$  and viscosity of 1.996, 0.590 Cp at 20  $^\circ\text{C}$ , respectively), the optical absorption spectra did not show the SPR peaks, similarly to the solutions containing Ag atoms. We irradiated these nanoparticle aggregates by nanoseconds laser pulses, which resulted in the appearance of well-defined SPR peaks for the Ag NPs. Fig. 2 shows the UV-Visible absorption spectra of NPs before and after laser irradiation. The laser ablation in liquids depends on the solvents density, viscosity, and absorption properties of ablated laser wavelength, as well as laser pulse energy and time of the ablation process [3,50–58]. In our case, instead of laser ablation of bulk metal targets in liquids, we have chosen a specific size of (100 nm, and 20 nm) aggregated/fragmented NPs in DMSO and toluene using laser irradiation at a fixed laser energy of 50 mJ and up to 30 min duration to investigate their NLO properties. The SPR peak values for disintegrated NPs of 100 nm and 20 nm in DMSO are 420 nm, 426 nm, whereas, in toluene 417 nm and 430 nm, respectively. The SEM

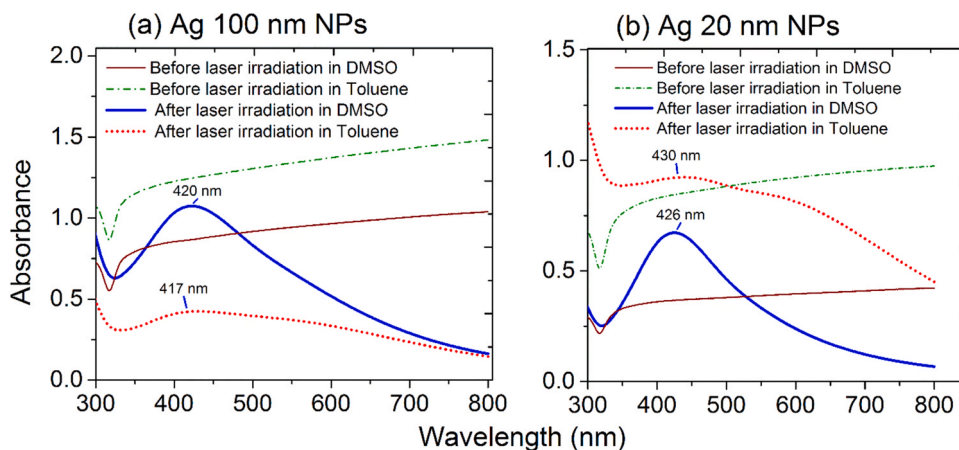


Fig. 2. Evolution of the optical extinction spectrum of NPs before and after laser radiation process in DMSO and toluene solvents for (a) Ag 100 nm NPs and (b) Ag 20 nm NPs, respectively.

images and SD of the irradiated Ag NPs for 100 nm and 20 nm are shown in Figs. 3 and 4, respectively. The aggregated Ag 100 nm and 20 nm NPs are disintegrated into mean size of 28 nm, 37 nm in DMSO and 23 nm, 33 nm in toluene, respectively. Ag 100 nm NPs were observed to break down their SD lower than 100 nm during laser irradiation. Whereas, in the case of Ag 20 nm NPs, initially these NPs are aggregated, which means the initial size is more than 20 nm i.e. integer multiples of 20 nm, which indicates that the smallest NPs are combined easily. Also, the surface volume of aggregated NPs of 20 nm is less as compared to 100 nm NPs, which leads to a decrease in the probability of interaction of 20 nm NPs with the irradiation laser pulse as compared to 100 nm NPs. Therefore, the disintegration of 100 nm NPs is more prominent, as a result, lower size NPs obtained. Moreover, the obtained results show that during the laser irradiation process the solvents which have high density and viscosity (DMSO) leads to a bigger size of NPs than the solvents of less density and viscosity (toluene). It inferred that lower viscosity and density of solvents allow high laser pulse energy to interact with the NPs and disintegrate them into a smaller size. In the present case, Ag NPs is spherical, clearly identified from the SEM images shown in Fig. 3. The difference of Ag NPs size changed their SPR peak positions, bandwidth and wavelength, and increased size shows a red shift in the absorption spectra (shown in Fig. 2), which directly affect third-order NLO properties of NPs.

### 3.2. Nonlinear absorption and refraction of Ag NPs suspensions in DMSO, and toluene

It is well known that Z-scan is an effective technique to measure the third-order NLO properties of the NPs suspensions. The values of the third-order nonlinear refraction index ( $n_2$ ) and nonlinear absorption coefficient ( $\beta$ ) for materials can be measured using the analysis of the Z-scan technique through CA and OA measurements, respectively. In the case of OA Z-scans, the 2PA, and SA induced normalized transmittance of laser pulses can be described by [59].

$$T_{2PA}(z) \approx 1 - \frac{q}{2\sqrt{2}} \quad (1)$$

$$T_{SA}(z) = 1 + \frac{I_0}{I_{sat}(x^2 + 1)} \quad (2)$$

Here,  $q(z) = I_0 \times \beta \times L_{eff} / (1 + z^2 / (z_0)^2)$ ,  $I_0$  is the peak intensity in the focal plane, and  $I_{sat}$  is the saturated intensity of the medium. In the case of CA Z-scan scheme, the normalized transmittance [T(z)] is related to the nonlinear refractive index by the following equation [60]:

$$T(z) = 1 + \frac{2(-\rho x^2 + 2x - 3\rho)\Delta\Phi_0}{(x^2 + 1)(x^2 + 9)} \quad (3)$$

Here  $x = z/z_0$ ,  $z_0 = kw_0^2$  is the Rayleigh length,  $k = 2\pi/\lambda$  is the wavenumber,  $w_0$  is the beam waist radius of the focused beam, and  $\Delta\Phi_0 = kn_2 I_0 L_{eff}$  is the phase change due to nonlinear refraction. The nonlinear refractive index is related to the phase change as  $n_2 = \Delta\Phi_0 / kL_{eff}I_0$ , where  $L_{eff} = [1 - \exp(-\alpha_0 L)] / \alpha_0$  is the effective length of the nonlinear medium and  $L$  is the sample thickness. The normalized transmittance curves from Eqs. (1) to (3) were used to fit the experimentally obtained data is shown in Fig. 5.

Fig. 5 shows the results of OA and CA measurements of pure solvents (DMSO and toluene) and disintegrated Ag NPs (contribution of pure solvents deducted) at  $I_0 = 1.4 \times 10^{11}$  W/cm<sup>2</sup>. In the process of disintegration of aggregated Ag 20 nm, the larger sized NPs (DMSO: 37 nm, toluene: 33 nm) are obtained when compared to irradiation of Ag 100 nm NPs (DMSO: 28 nm, toluene: 23 nm). The

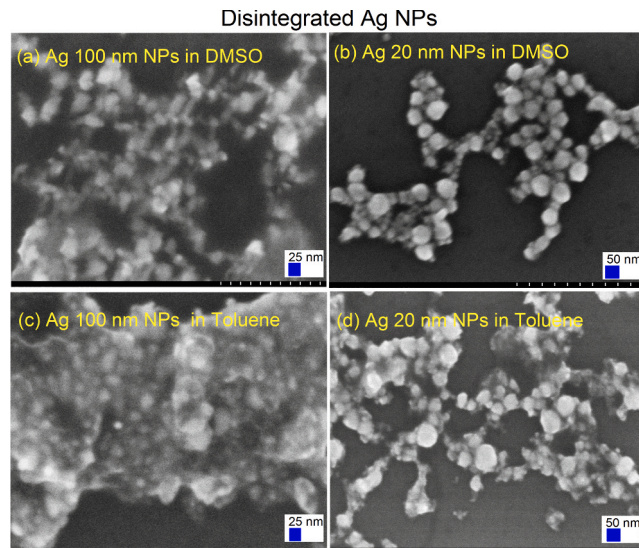


Fig. 3. HR-SEMs images of (a, c) Ag 100 nm and (b, d) 20 nm suspensions after irradiation process in DMSO, and toluene, respectively.

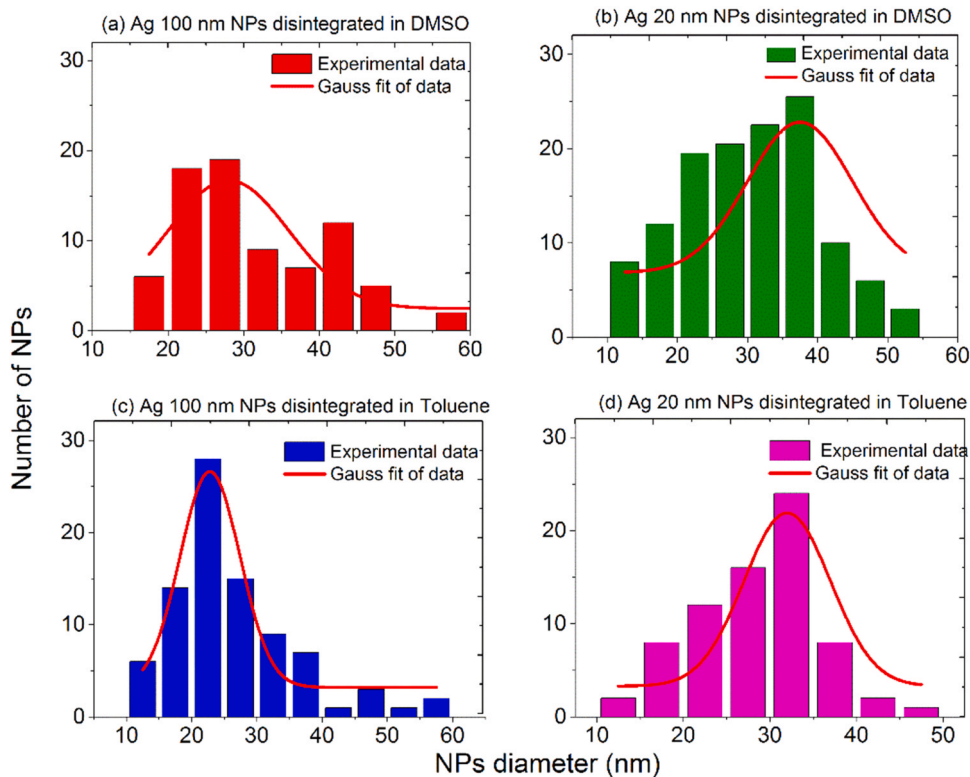


Fig. 4. The SD range of Ag NPs (obtained from SEM images) for (a,c) Ag 100 nm and (b,d) 20 nm suspensions through the process of irradiation in DMSO, and toluene, respectively.

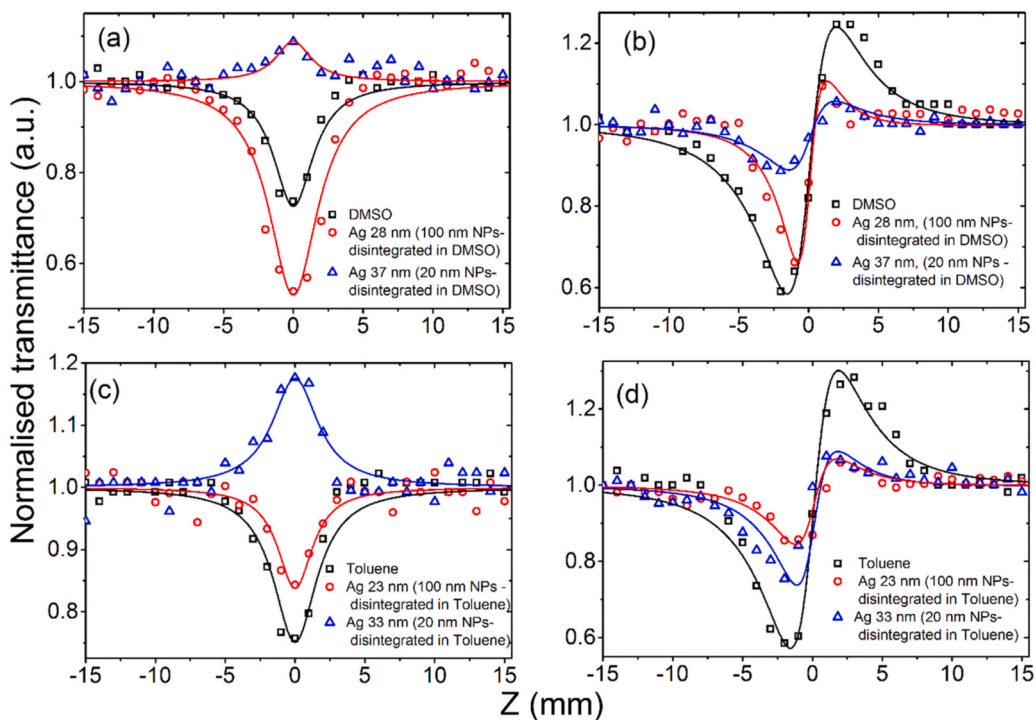


Fig. 5. OA and CA measurements of pure solvents and NPs obtained after the disintegration of 100 nm and 20 nm NPs in DMSO and toluene, respectively. In the case of NPs solutions, the contribution of pure solvents was deducted.

mean size, SD and NLO coefficients of produced NPs is shown in Table 1. It was observed that larger-sized Ag NPs 37 nm and 33 nm possess SA, whereas, 28 nm and 23 nm possess RSA (2PA) at off-resonant wavelength 800 nm. There have been several reports on the increase in the 2PA coefficient with an increase in the size of NPs and SA switching to RSA, due to size, shape and intensity of the input laser pulses [36,61–70]. In saturable absorber NPs, light absorption decreases with increase in incident light intensity and whereas for RSA, NPs transmit less with increase in intensity. As prepared Ag NPs show a difference in the peak maxima, plasmon bandwidth and SPR wavelength, and redshift in their peak values (shown in Fig. 2) with increasing the size of NPs. As the size of Ag NPs increases, the localized SPR (LSPR) effect gradually decreases and light scattering becomes more dominant [69], and leads to saturation of excited state or bleaching of the ground state through intraband  $sp \rightarrow sp$  transition (scheme 1, Fig. 6), whereas, the smaller Ag NPs have strong LSPR effect which leads to free carrier absorption or multiphoton absorption causes the RSA (2PA) through intraband  $sp \rightarrow sp$  transition (scheme 2, Fig. 6) at off-resonant excitation wavelength 800 nm. Thus, the LSPR effect has a great impact on the absorbance of NPs, which directly depends on the size of NPs. It was reported in the above-mentioned references [36,61–70] that 2PA was observed for Ag NPs as the size decrease whereas SA was observed for a larger size which was found to be in good agreement with our reported data. As our data suggest that as smaller sizes NPs exhibit only RSA and SA is negligible, we can conclude that 2PA (@ 800 nm) process is the obvious mechanism for smaller size NPs. Table 2 illustrates the NLO response from various NPs with a variation of their sizes. This nonlinear optical response arises from inter and intraband electronic excitation involving  $sp$  bands and inner  $d$ -orbital bands associated with metal NPs.

In the case of CA Z-scan measurements, the Ag NPs in DMSO and toluene exhibit self-focusing having a positive coefficient of nonlinear refraction. There have been several reports with pioneer work by M. Sheik-Bahae et al. [74], for the self-focusing effect using low repetition rate laser pulses for molecule/nanoparticle. The self-focusing effect is the response of the refractive index of the material upon interaction with intense laser pulses which depends on the repetition rate of the laser pulses. Nonlinear index of refraction under high influence of fs laser pulses at low repetition rate exhibit self-focusing which is related to the dissipation of thermal load on NPs. Since the repetition rate of laser pulses used in the experiment was 1 kHz which provide a sufficient amount of time for the nanoparticle to dissipate the thermal load exerted by a laser pulse. Hence NPs under the 1 kHz femtosecond laser pulses show a self-focusing effect. Consequently, DMSO exhibits strong nonlinear refraction with self-focusing ( $n_2 = 14.7 \times 10^{-16} \text{ cm}^2/\text{W}$ ) and 2PA ( $\beta = 5.61 \times 10^{-11} \text{ cm}^2/\text{W}$ ), which results in an asymmetric nonlinear transmittance curve as shown in Fig. 5(b). CA Z-scan profile for DMSO and toluene is asymmetric due to the influence of 2PA in the solvent, in addition to the positive nonlinear refraction.

The obtained  $n_2$  values of Ag 23 nm (100 nm NPs disintegrated in toluene), 28 nm (100 nm NPs disintegrated in DMSO), 33 nm (20 nm NPs disintegrated in DMSO) and 37 nm (20 nm NPs disintegrated in toluene) are found to be 4.9, 9.6, 7.6 and  $3.7 \times 10^{-16} \text{ cm}^2/\text{W}$ , respectively. These values indicate that the nonlinear refraction increases with decreasing the size of NPs. However, it was observed that unlike Ag NPs in toluene, the self-focusing effect in DMSO decreases as the size of Ag NPs increases shown in Fig. 5(b and d). The intense laser pulse creates thermal load on the Ag NPs upon interaction, which creates the self-defocusing effect at low repetition rate of laser pulses. This occurs via transfer of heat from Ag NPs to the solvent. The self-defocusing effect is directly related with the shape and size of the NPs. Specific heat capacity ( $C_p$ ) for NPs decreases as the size of NPs increases [68]. It implies that NPs with larger sizes will transfer a large part of thermal load to the solvent, which eventually creates the self-defocusing effect by reducing the solvent refractive index in the vicinity of the focal volume. Self-defocusing influences the nonlinear optical response of the NPs solution in DMSO. Another solvent (toluene) exhibits very small nonlinear refraction ( $n_2 = 0.16 \times 10^{-16} \text{ cm}^2/\text{W}$ ) as compared with DMSO ( $n_2 = 14.7 \times 10^{-16} \text{ cm}^2/\text{W}$ ), which is demonstrated by the symmetric nonlinear transmittance curve in Fig. 5(d). The dissipation of thermal load on the solvent molecule from intense fs laser pulses depends on the thermal conduction time ( $\tau = \frac{\omega_0^2 \rho c_p}{4k}$ ), where  $\omega_0$  is beam waist at focus,  $\rho$  is the density of solvent,  $c_p$  is the specific heat capacity and  $k$  is the thermal conductivity. As shown in the following Table 3, the thermal conduction time for toluene was found to be shorter than for DMSO, which leads smaller thermal load in toluene as compared to DMSO. Hence, the self-focusing effect was more prominent in DMSO than toluene.

We have measured the NLO response of pure solvents and NPs containing solvents. We deducted the contribution of pure solvents effect and presented the results in Fig. 5, which includes the open and closed apertures Z-scans of pure solvents. The average data of the experiments repeated a few times are presented. It was observed that in five measurements of repeated experiments at different positions on the aqueous solutions the Z-scan curves were similar. However, even though we have successfully disintegrated the NPs in DMSO and toluene, the closed-aperture Z-scans shown in Fig. 5(b) demonstrate some asymmetric curves for DMSO. As mentioned above, we deducted the NLO contribution of this pure solvent. It is also assumed that the slight effect of polymerization is negligible and NLO properties of NPs mainly depend on their SD. The Ag NPs with different sizes and shapes, it may be possible to use these materials for various optical applications such as laser pulse compression and OL for protecting optical sensors from high power laser pulses [47]. After measuring the third-order NLO properties of disintegrated Ag NPs, we focused our study on the plasma plume of bulk

**Table 1**  
Summary of NLO properties of Ag NPs.

At Input laser intensity $I_0 = 1.4 \times 10^{11} \text{ (W/cm}^2\text{)}$	Obtained SD/mean (nm)	$\beta \text{ (cm/W)} \times 10^{-11}$	$n_2 \text{ (cm}^2\text{/W)} \times 10^{-16}$	$I_{\text{sat}} \text{ (W/cm}^2\text{)} \times 10^{11}$
DMSO	–	5.61	14.7	
Ag 100 nm, DMSO	10–60 (28)	9.61	9.6	
Ag 20 nm, DMSO	10–60 (37)	–	3.7	15.5
Toluene	–	5.09	0.16	
Ag 100 nm, Toluene	10–60 (23)	3.32	4.9	
Ag 20 nm, Toluene	10–60 (33)	–	7.6	:

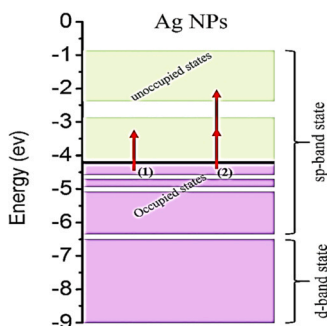


Fig. 6. Excitation mechanism in Ag NPs during 800 nm excitation.

Table 2

Summary of NLO properties for recently reported other metal NPs.

NPs	Preparation method	Average size of NPs	$\lambda$ (nm)	NLO process	Nonlinear values		Ref.
					$I_{SA}$ (GW/cm <sup>2</sup> )	$\beta$ (cm/GW)	
Au-PPA	Nano sphere lithography	37 nm 70 nm	800	TPA + SA		54 29	[71]
Au-CdSe	solution	3.37 nm 5.07 nm	532	SA+RSA		98 14	[72]
Ag NPs	Chemical reduction method	30 nm 37 nm	800	SA+RSA	830 270	$1.7 \times 10^{-2}$ $4.6 \times 10^{-2}$	[36]
Ag /PVP	Chemical reduction method	17.5 nm	400	RSA		$8.2 \times 10^{-3}$	[73]

Table 3

Thermophysical properties of pure solvents.

Solvent	$C_p$ (J/g/K)	$k$ (Wcm <sup>-1</sup> K <sup>-1</sup> )	$\rho$ (g/cm <sup>3</sup> )	thermal conduction time ( $\tau = \frac{\omega_0^2 \rho C_p}{4k}$ ), in ms
DMSO	1.966	18.6	1.0955	16.8
Toluene	1.595	13.2	0.8669	15.2

Ag and original Ag NPs for a THG.

3.3. THG produced from plasma plumes of Ag targets

THG from plasma can be used as probe radiation to characterize the plasma components. Earlier, extensively studied the

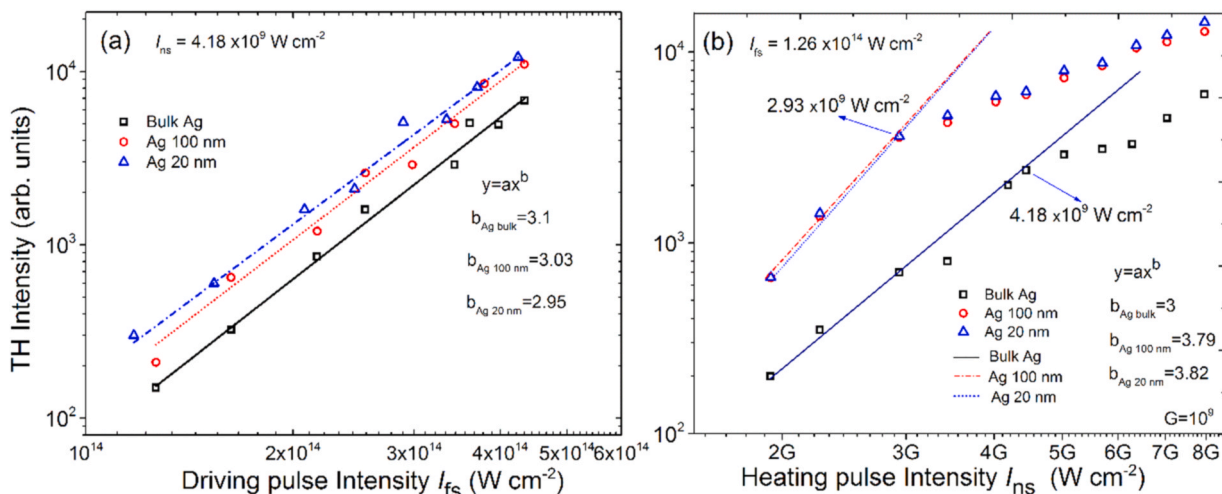


Fig. 7. Dependence of TH's intensity on heating (ablation) pulse intensities.

spatiotemporal profile of generated particles in various plasmas produced from bulk targets (C, Cr, In, Ni, Ag, CdS and ZnS) using pulsed laser ablation and THG using 800 nm, 40 fs probe pulses [75]. The generation of lower-order harmonics depends on the contribution of particles with lower mass ejected from the targets during the ablation process. The velocity of NPs depends on the mass of ejected particles and the fluence of the HP [76]. Fig. 7(a, b) shows the yield of TH intensity for Ag bulk and NPs of 100 nm, and 20 nm at fixed ns HP intensity  $I_{ns} = 4.18 \times 10^{10}$  W/cm<sup>2</sup> and  $I_{fs} = 1.26 \times 10^{14}$  W/cm<sup>2</sup> with respect to change in the intensities of DP and HP, respectively. TH yield data are fitted with the power equation  $y = ax^b$ , where  $b$  is the power order. The TH yield shows cubic dependence for DP intensities for all samples, as well as the similar behavior is observed for ns HP intensities up to  $I_{ns} = 4.18 \times 10^9$  W/cm<sup>2</sup> for bulk ( $b=3$ ) and  $2.93 \times 10^9$  W/cm<sup>2</sup> for Ag 100 nm ( $b = 3.79$ ) and Ag 20 nm ( $b = 3.82$ ). After this intensity of ns HP, the plasma plume might get saturation and TH yield shows the deviation from the cubic fit as shown in Fig. 7(b). It indicates that NPs plasma gets saturation, earlier than bulk Ag of plasma. However, the intensities of TH signal for NPs higher than Ag bulk, which might be due to denser plasma plume of NPs at similar ns pulse intensity. It has been predicted that in the plasma of Ag, atoms, ions, small clusters and their compositions are mostly responsible for the generation of efficient TH intensity [77].

THG in air and laser-produced plasmas (LPPs) using femtosecond pulses from Ti: sapphire class lasers is a well-studied process that allows determining the maximally available conversion efficiency of this NLO effect and diminishing the impeding mechanisms restricting this process [78,79]. THG serves as a tool for ~266 nm sources of fs pulses at the conversion efficiency from 800-nm class lasers of up to  $10^{-3}$  or even higher [80,81]. Earlier and present work demonstrates that TH signal generated from Ag plasma plumes has the highest yield than the other materials [75]. Therefore, the generated TH signal is sufficient for various applications of these UV sources in spectroscopy, photo modification of sensitive organic materials, photoluminescent studies of dyes and complex molecules. THG in LPP has already attracted attention due to its interesting features that allow determining plasma characteristics and determination of the optimal ablating materials for further expansion of generating harmonics towards the extreme ultraviolet region through HHG [82].

It is known that the plasma plume contains both neutral and charged atoms/NPs and they both may contribute to the observed third and higher-order harmonics spectra. Therefore, we have attempted to find the ionization probability of Ag atom and Ag<sup>+</sup> ions [83]. According to the Lewenstein model [84], HHG is a three-step process: (i) ionization by the strong laser field, (ii) acceleration in the laser field, and (iii) recombination with the parent ion and emission of a high energy photon. Therefore, to generate high harmonics it is crucial to have a sufficiently intense laser field that is capable to ionize the target atom/ion. To estimate the ionization probability of Ag atom (ionization potential = 7.48 eV) and Ag<sup>+</sup> ion (ionization potential = 21.48 eV) by the DP, we used the Perelomov-Popov-Terent'ev (PPT) formula of ionization rate [85], which is applicable for ionization of various atoms in both multiphoton and tunnelling regime [86]. As shown in Fig. 8, the calculated ionization probability of Ag atom and Ag<sup>+</sup> approaches one (saturation) when the laser intensity reaches  $2 \times 10^{13}$  W/cm<sup>2</sup> and  $3 \times 10^{14}$  W/cm<sup>2</sup>, respectively. Even at  $1.8 \times 10^{14}$  W/cm<sup>2</sup> (the lowest DP intensity we used shown in Fig. 7(a)), the ionization probability of Ag<sup>+</sup> is about 0.4, which is still significant. However, it is noteworthy that even at high intensities where both of the ionization probabilities for Ag atom and Ag<sup>+</sup> saturate, the total number of ionization events in the entire interaction region should be more for Ag atom than for Ag<sup>+</sup>. It is because the spatial distribution of the DP intensity has a Gaussian profile, so the outer part of the laser beam has much lower intensities than the measured peak intensity and so may not be sufficient to ionize Ag<sup>+</sup>. Nevertheless, to obtain a good estimate of the relative contribution between Ag and Ag<sup>+</sup>, one needs to also know the number density of the atoms and ions, the corresponding recombination probabilities, etc. But, at least the contribution from Ag<sup>+</sup> is likely to be non-negligible compared with Ag in most of the data set presented above in Fig. 7.

#### 4. Conclusions

In conclusion, the paper reports the third-order NLO properties such as nonlinear absorption and refraction coefficients of Ag NPs of sizes 23–37 nm range, which is produced from commercially available Ag NPs of sizes 100 nm, and 20 nm using laser irradiation. The different SD of these NPs was achieved using the laser irradiation process through nanoseconds 1064 nm wavelengths in two solvents (DMSO and toluene). The aggregated NPs can be disintegrated into small size NPs in the presence of low viscous and density of solvents during the laser irradiation. In the present study, the Z-scan measurements show the larger size NPs (> 30 nm) possess saturable absorption, whereas small-sized NPs (< 30 nm) show two-photon absorption. The Ag NPs with different sizes and shapes, it may be possible to use these materials for various optical applications such as laser pulse compression and optical limiting for protecting optical sensors from high power laser pulses. The third-order harmonic emitted from the plasma plume of Ag NPs possess higher intensity compares to the plasma plume of Ag bulk, among NPs, the smallest NPs i.e. Ag 20 nm produce higher intensity as compared to 100 nm NPs. Finally, we have calculated the ionization probability of Ag and Ag<sup>+</sup>, which approaches one (saturation) when the laser intensity reaches  $2 \times 10^{13}$  W/cm<sup>2</sup> and  $3 \times 10^{14}$  W/cm<sup>2</sup>, respectively. This confirms that the third harmonic emitted due to the plasma plume components such as atoms and neutral particles at a lower intensity of driving pulses, and at a higher intensity of driving pulses which includes the Ag<sup>+</sup> ions. THG in laser-produced plasmas of Ag has attracted attention due to its ionization probability that determining plasma characteristics, with respect to optimal driving and heating pulse intensities. The studies of THG and ionization probability calculations useful for further expansion of generating harmonics towards the extreme ultraviolet region through high-order harmonics generation from Ag plasma plumes.

#### Funding

The research was funded by the Chinese Academy of Sciences President's International Fellowship Initiative. Grant No. 2021PM0036, National Natural Science Foundation of China (91750205, 61774155), K.C. Wong Education Foundation (GJTD-2018-

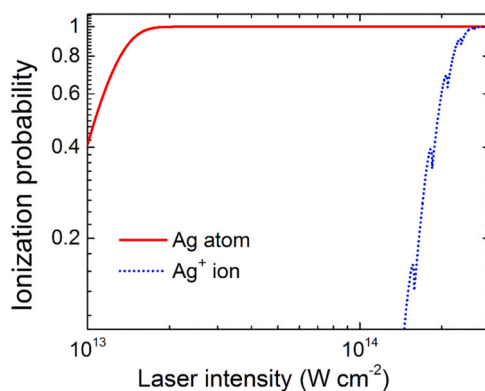


Fig. 8. Laser intensity dependence of calculated ionization probability of neutral Ag atom and Ag<sup>+</sup> ion irradiated by 800 nm 35 fs pulse using the PPT formula [85].

08), National Key Research and Development Program of China (2017YFB1104700, 2018YFB1107202), Jilin Provincial Science & Technology Development Project (20180414019GH), European Regional Development Fund (1.1.1.5/19/A/003), and The Key Program of the International Partnership Program of CAS (181722KYSB20160015).

### Declaration of Competing Interest

The authors declare that they have no conflict of interest.

### References

- [1] M. Priyadarshini, J.N. Acharyya, S. Mahajan, G. Vijaya Prakash, Optical nonlinearities in chemically synthesized and femtosecond laser fabricated gold nanoparticle colloidal solutions, *Opt. Laser Technol.* 139 (2021), 107008, <https://doi.org/10.1016/j.optlastec.2021.107008>.
- [2] M.S.S. Bharati, C. Byram, V.R. Soma, Femtosecond laser fabricated Ag@Au and Cu@Au alloy nanoparticles for surface enhanced raman spectroscopy based trace explosives detection, *Front. Phys.* 6 (2018) 1–13, <https://doi.org/10.3389/fphy.2018.00028>.
- [3] Forsythe R.C., Cox C.P., Wilsey M.K., Mu A.M., Pulsed Laser in Liquids Made Nanomaterials for Catalysis, *Chem. Rev.*, doi:10.1021/acs.chemrev.0c01069.
- [4] R. Li, N. Dong, F. Ren, H. Amekura, J. Wang, F. Chen, Nonlinear absorption response correlated to embedded ag nanoparticles in BGO single crystal: from two-photon to three-photon absorption, *Sci. Rep.* 8 (2018) 4–11, <https://doi.org/10.1038/s41598-018-20446-6>.
- [5] M.G. Manera, A. Colombelli, A. Taurino, A.G. Martin, R. Rella, Magneto-Optical properties of noble-metal nanostructures: functional nanomaterials for bio sensing, *Sci. Rep.* 8 (2018) 1–12, <https://doi.org/10.1038/s41598-018-30862-3>.
- [6] K.S. Rao, R.A. Ganeev, K. Zhang, Y. Fu, G.S. Boltaev, P. Krishnendu, P.V. Redkin, C. Guo, Laser ablation – induced synthesis and nonlinear optical characterization of titanium and cobalt nanoparticles, *J. Nanopart. Res* 20 (20) (2018) 285, <https://doi.org/10.1007/s11051-018-4391-3>.
- [7] J. Natsuki, A review of silver nanoparticles: synthesis methods, properties and applications, *IJMSA* 4 (2015) 325, <https://doi.org/10.11648/j.ijmsa.20150405.17>.
- [8] S.A. Jilil, B. Lai, M. Elkabbash, J. Zhang, E.M. Garcell, Subhash C. Singh, C. Guo, Spectral absorption control of femtosecond laser-treated metals and application in solar-thermal devices, *Light Sci. Appl.* 9 (2020) 14, <https://doi.org/10.1038/s41377-020-0242-y>.
- [9] J. Zhang, M. Elkabbash, Ran Wei, Subhash C. Singh, B. Lam, C. Guo, Plasmonic metasurfaces with 42.3% transmission efficiency in the visible, *Light Sci. Appl.* 8 (2019) 53, <https://doi.org/10.1038/s41377-019-0164-8>.
- [10] U. Yesilgul, F. Urgan, S. Sakiroglu, H. Sari, E. Kasapoglu, I. Sökmen, Nonlinear optical properties of a semi-exponential quantum wells: effect of high-frequency intense laser field, *Opt. (Stuttg.)* 185 (2019) 311–316, <https://doi.org/10.1016/j.ijleo.2019.03.126>.
- [11] G. Ma, Y. Yao, X. Zhang, S. Wang, Nonlinear optical properties of tungsten disulfide as saturable absorber based on Q-switched fiber laser, *Optik* 198 (2019), 163251, <https://doi.org/10.1016/j.ijleo.2019.163251>.
- [12] F. Urgan, M.K. Bahar, M.G. Barseghyan, L.M. Pérez, D. Laroze, Effect of intense laser and electric fields on nonlinear optical properties of cylindrical quantum dot with Morse potential, *Optik* 236 (2021), 166621, <https://doi.org/10.1016/j.ijleo.2021.166621>.
- [13] K. Erturk, S. Isik, O. Aras, Y. Kaya, Investigation of structural, spectral, optical and nonlinear optical properties of nanocrystal CdS: electrodeposition and quantum mechanical studies, *Optik* 243 (2021), 167469, <https://doi.org/10.1016/j.ijleo.2021.167469>.
- [14] L. Xu, Y.Y. Wang, J. Huang, C.Y. Chen, Z.X. Wang, H. Xie, Silver nanoparticles: synthesis, medical applications and biosafety, *Theranostics* 10 (2020) 8996–9031, <https://doi.org/10.7150/thno.45413>.
- [15] M.S. Satya Bharati, B. Chandu, S.V. Rao, Explosives sensing using Ag-Cu alloy nanoparticles synthesized by femtosecond laser ablation and irradiation, *RSC Adv.* 9 (2019) 1517–1525, <https://doi.org/10.1039/C8RA08462A>.
- [16] S. Qu, Y. Zhang, H. Li, J. Qiu, C. Zhu, Nanosecond nonlinear absorption in Au and Ag nanoparticles precipitated glasses induced by a femtosecond laser, *Opt. Mater. (Amst.)* 28 (2006) 259–265, <https://doi.org/10.1016/j.optmat.2005.01.011>.
- [17] R. Rangel-Rojo, J. McCarthy, H.T. Bookey, A.K. Kar, L. Rodriguez-Fernandez, J.C. Cheang-Wong, A. Crespo-Sosa, A. Lopez-Suarez, A. Oliver, V. Rodriguez-Iglesias, H.G. Silva-Pereyra, Anisotropy in the nonlinear absorption of elongated silver nanoparticles in silica, probed by femtosecond pulses, *Opt. Commun.* 282 (2009) 1909–1912, <https://doi.org/10.1016/j.optcom.2009.01.048>.
- [18] K. Furusawa, K. Takahashi, H. Kumagai, K. Midorikawa, M. Obara, Ablation characteristics of Au, Ag, and Cu metals using a femtosecond Ti:sapphire laser, *Appl. Phys. A* 69 (1999) S359–S366, <https://doi.org/10.1007/s003390051417>.
- [19] K.X. Zhang, Y. Cai, C.B. Yao, X. Wen, Y. Han, H.T. Yin, W.J. Sun, Q.H. Li, Structures, growth mechanism and optical properties of Ag-ZnO cored nanotubes, *Mater. Lett.* 234 (2019) 191–195, <https://doi.org/10.1016/j.matlet.2018.09.100>.
- [20] H.-Q. Liu, C.-B. Yao, G.-Q. Jiang, Y. Cai, Synthesis, structure and ultrafast nonlinear absorption properties of ZnO-time/MoS2 films, *J. Alloy. Compd.* 847 (2020), 156524, <https://doi.org/10.1016/j.jallcom.2020.156524>.
- [21] A. Sakthisabarimoorathi, M. Jose, S.A. Martin Britto Dhas, S. Jerome Das, Fabrication of Cu@Ag core-shell nanoparticles for nonlinear optical applications, *J. Mater. Sci. Mater. Electron.* 28 (2017) 4545–4552, <https://doi.org/10.1007/s10854-016-6090-0>.

- [22] Q. Ouyang, K. Zhang, W. Chen, F. Zhou, W. Ji, Nonlinear absorption and nonlinear refraction in a chemical vapor deposition-grown, ultrathin hexagonal boron nitride film, 1368-71, *Opt. Lett.* 41 (2016), <https://doi.org/10.1364/ol.41.001368>.
- [23] K.X. Zhang, C.B. Yao, X. Wen, Q.H. Li, W.J. Sun, Ultrafast nonlinear optical properties and carrier dynamics of silver nanoparticle-decorated ZnO nanowires, *RSC Adv.* 8 (2018) 26133–26143, <https://doi.org/10.1039/c8ra03027h>.
- [24] Z. Dehghani, E. Saievar Iranizad, M. Nadafan, Investigation of electric field effect on the third order nonlinear optical properties of Fe3O4 nanoparticles-doped nematic liquid crystal, *Opt. Commun.* 334 (2015) 16–21, <https://doi.org/10.1016/j.optcom.2014.07.058>.
- [25] M. Nadafan, R. Malekfar, Z. Dehghani, Microstructural and nonlinear optical properties of SiO2 and Al2O3 nanoparticles doped in polyurethane, *J. Mater. Res.* 30 (2015) 1788–1796, <https://doi.org/10.1557/jmr.2015.101>.
- [26] M. Nadafan, M. Parishani, Z. Dehghani, J.Z. Anvari, R. Malekfar, Third-order nonlinear optical properties of NiFe2O4 nanoparticles by Z-scan technique, *Opt. (Stuttg.)* 144 (2017) 672–678, <https://doi.org/10.1016/j.jleleo.2017.06.128>.
- [27] N. Faraji, W.M.M. Yunus, A. Kharazmi, E. Saion, M. Shahmiri, N. Tamchek, Synthesis, characterization and nonlinear optical properties of silver / PVA nanocomposites, *JEOS:RP* 7 (2012), 12040, <https://doi.org/10.2971/jeos.2012.12040>.
- [28] A.A. Mitiku, B. Yilma, Review article a review on green synthesis and antibacterial activity of silver nanoparticles, *Int. J. Pharm. Sci. Rev. Res.* 46 (2017) 52–57.
- [29] M. Rothe, Y. Zhao, G. Kewes, Z. Kochovski, W. Sigle, P.A. van Aken, C. Koch, M. Ballauff, Y. Lu, O. Benson, Silver nanowires with optimized silica coating as versatile plasmonic resonators, *Sci. Rep.* 9 (2019) 1–12, <https://doi.org/10.1038/s41598-019-40380-5>.
- [30] E.J. Guidelli, O. Baffa, D.R. Clarke, Enhanced UV emission from silver/ZnO and Gold/ZnO core-shell nanoparticles: photoluminescence, radioluminescence, and optically stimulated luminescence, *Sci. Rep.* 5 (2015) 1–11, <https://doi.org/10.1038/srep14004>.
- [31] V. Thamilselvi, K.V. Radha, A review on the diverse application of silver nanoparticle, *IOSR J. Pharm.* 07 (2017) 21–27, <https://doi.org/10.9790/3013-0701012127>.
- [32] J.H. Byeon, Y.W. Kim, A novel polyol method to synthesize colloidal silver nanoparticles by ultrasonic irradiation, *Ultrason. Sonochem.* 19 (2012) 209–215, <https://doi.org/10.1016/j.ultrasonch.2011.06.004>.
- [33] S.I. Dolgaev, A.V. Simakin, V.V. Voronov, G.A. Shafeev, F. Bozon-verduraz, Nanoparticles produced by laser ablation of solids in liquid environment, *Appl. Surf. Sci.* 186 (2002) 546–551, [https://doi.org/10.1016/S0169-4332\(01\)00634-1](https://doi.org/10.1016/S0169-4332(01)00634-1).
- [34] A.S. Nikolov, R.G. Nikov, I.G. Dimitrov, N.N. Nedyalkov, P.A. Atanasov, M.T. Alexandrov, D.B. Karashanova, Modification of the silver nanoparticles size-distribution by means of laser light irradiation of their water suspensions, *Appl. Surf. Sci.* 280 (2013) 55–59, <https://doi.org/10.1016/j.apsusc.2013.04.079>.
- [35] G.S. Boltsev, R.A. Ganeev, P.S. Krishnendu, S.K. Maurya, P.V. Redkin, K.S. Rao, K. Zhang, C. Guo, Strong third-order optical nonlinearities of Ag nanoparticles synthesized by laser ablation of bulk silver in water and air, *Appl. Phys. A* 124 (2018) 766, <https://doi.org/10.1007/s00339-018-2195-z>.
- [36] S.K. Maurya, A. Rout, R.A. Ganeev, C. Guo, Effect of size on the saturable absorption and reverse saturable absorption in silver nanoparticle and ultrafast dynamics at 400nm, *J. Nanomater* 2019 (2019), 9686913, <https://doi.org/10.1155/2019/9686913>.
- [37] A. Zielińska, E. Skwarek, A. Zaleska, M. Gazda, J. Hupka, Preparation of silver nanoparticles with controlled particle size, *Procedia Chem.* 1 (2009) 1560–1566, <https://doi.org/10.1016/j.proche.2009.11.004>.
- [38] T. Tsuji, D.H. Thang, Y. Okazaki, M. Nakanishi, Y. Tsuboi, M. Tsuji, Preparation of silver nanoparticles by laser ablation in polyvinylpyrrolidone solutions, *Appl. Surf. Sci.* 254 (2008) 5224–5230, <https://doi.org/10.1016/j.apsusc.2008.02.048>.
- [39] M. Ali, N. Remali, F. Yehya, A.K. Chaudhary, V.V.S.S. Srikanth, Picosecond laser induced fragmentation of coarse Cu2O particles into nanoparticles in liquid media, *Appl. Surf. Sci.* 357 (2015) 1601–1605, <https://doi.org/10.1016/j.apsusc.2015.10.041>.
- [40] M. Hari, S. Mathew, B. Nithyaja, S.A. Joseph, V.P.N. Nampoori, P. Radhakrishnan, Saturable and reverse saturable absorption in aqueous silver nanoparticles at off-resonant wavelength, *Opt. Quantum Electron.* 43 (2012) 49–58, <https://doi.org/10.1007/s11082-011-9502-7>.
- [41] B.H. Yu, D.L. Zhang, Y. Bin Li, Q. Bin Tang, Nonlinear optical behaviors in a silver nanoparticle array at different wavelengths, *Chin. Phys. B* 22 (2013), 014212, <https://doi.org/10.1088/1674-1056/22/1/014212>.
- [42] Y.X. Zhang, Y.H. Wang, Nonlinear optical properties of metal nanoparticles: a review, *RSC Adv.* 7 (2017) 45129–45144, <https://doi.org/10.1039/c7ra07551k>.
- [43] J. Jayabalan, A. Singh, R. Chari, S.M. Oak, Ultrafast third-order nonlinearity of silver nanospheres and nanodiscs, *Nanotechnology* 18 (2007), 315704, <https://doi.org/10.1088/0957-4484/18/31/315704>.
- [44] C. Zheng, W. Li, W. Chen, X. Ye, Nonlinear optical behavior of silver nanopentagons, *Mater. Lett.* 116 (2014) 1–4, <https://doi.org/10.1016/j.matlet.2013.10.101>.
- [45] A. Ajami, W. Husinsky, B. Svecova, S. Vytlykacova, P. Nekvindova, Saturable absorption of silver nanoparticles in glass for femtosecond laser pulses at 400nm, *J. Non Cryst. Solids* 426 (2015) 159–163, <https://doi.org/10.1016/j.jnoncrysol.2015.06.027>.
- [46] Y. Gao, W. Wu, D. Kong, L. Ran, Q. Chang, H. Ye, Femtosecond nonlinear absorption of Ag nanoparticles at surface plasmon resonance, *Phys. E Low. Dimens. Syst. Nanostruct.* 45 (2012) 162–165, <https://doi.org/10.1016/j.physe.2012.07.023>.
- [47] U. Gurudas, E. Brooks, D.M. Bubb, S. Heiroth, T. Lippert, A. Wokaun, Saturable and reverse saturable absorption in silver nanodots at 532 nm using picosecond laser pulses, *J. Appl. Phys.* 104 (2008), 073107, <https://doi.org/10.1063/1.2990056> (1-8-8-8).
- [48] R. Philip, P. Chantharasupawong, H. Qian, R. Jin, J. Thomas, Evolution of nonlinear optical properties: from gold atomic clusters to plasmonic nanocrystals, *Nano Lett.* 12 (2012) 4661–4667, <https://doi.org/10.1021/nl301988v>.
- [49] K.-S. Lee, M.A. El-Sayed, Gold and silver nanoparticles in sensing and imaging: sensitivity of plasmon response to size, shape, and metal composition, *J. Phys. Chem. B* 110 (2006) 19220–19225, <https://doi.org/10.1021/jp062536y>.
- [50] A.R. Sadrolhossein, M.A. Mahdi, F. Alizadeh, S.A. Rashid, Chapter 4: Laser Ablation Technique for Synthesis of Metal Nanoparticle in Liquid. *Laser Technology its Applied Biomaterials, Intech.*, 2013, pp. 62–84, <https://doi.org/10.5772/intechopen.80374>.
- [51] S. Reich, A. Letzel, A. Menzel, N. Kretschmar, B. Gökce, S. Barcikowski, A. Plech, Early appearance of crystalline nanoparticles in pulsed laser ablation in liquids dynamics, *Nanoscale* 11 (2019) 6962–6969, <https://doi.org/10.1039/c9nr01203f>.
- [52] N.F. Villegas Borrero, J.M. Clemente da Silva Filho, V.A. Ermakov, F.C. Marques, Silver nanoparticles produced by laser ablation for a study on the effect of SERS with low laser power on N719 dye and Rhodamine-B, *MRS Adv.* 4 (2019) 723–731, <https://doi.org/10.1557/adv.2019.157>.
- [53] M.I. Ismael, G.G. Ali, U. Muhsin Nayef, Characterization of silver nanoparticles on porous silicon by laser ablation in liquid, *IOP Conf. Ser. Mater. Sci. Eng.* 1126 (2021), 012006, <https://doi.org/10.1088/1757-899x/1126/1/012006>.
- [54] M. Ratti, J.J. Nadeo, J.C. Griepenburg, S.M. O'Malley, D.M. Bubb, E.A. Klein, Production of metal nanoparticles by pulsed laser-ablation in liquids: a tool for studying the antibacterial properties of nanoparticles, *J. Vis. Exp.* 2017 (2017) 1–8, <https://doi.org/10.3791/55416>.
- [55] E.A. Ganash, R.M. Altuwirqi, Size control of synthesized silver nanoparticles by simultaneous chemical reduction and laser fragmentation in Origanum majorana extract: Antibacterial application, in: *Materials (Basel)*, 2021, p. 2326, <https://doi.org/10.3390/ma14092326>.
- [56] Y. Yu, L. Yan, M. Yue, H. Xu, Femtosecond laser-assisted synthesis of silver nanoparticles and reduced graphene oxide hybrid for optical limiting, *R. Soc. Open Sci.* 5 (2018), 171436, <https://doi.org/10.1098/rsos.171436>.
- [57] A.A. Menazea, Femtosecond laser ablation-assisted synthesis of silver nanoparticles in organic and inorganic liquids medium and their antibacterial efficiency, *Radiat. Phys. Chem.* 168 (2020), 108616, <https://doi.org/10.1016/j.radphyschem.2019.108616>.
- [58] H. Du, V. Castaing, D. Guo, B. Viana, Rare-earth doped-nanoparticles prepared by pulsed laser ablation in liquids, *Ceram. Int.* 46 (2020) 26299–26308, <https://doi.org/10.1016/j.ceramint.2020.04.291>.
- [59] M. Sheik-Bahae, A.A. Said, T.H. Wei, D.J. Hagan, E.W. Van Stryland, Sensitive measurement of optical nonlinearities using a single beam, *IEEE J. Quantum Electron* 26 (1990) 760–769, <https://doi.org/10.1109/3.53394>.
- [60] X. Liu, S. Guo, H. Wang, L. Hou, Theoretical study on the closed-aperture Z-scan curves in the materials with nonlinear refraction and strong nonlinear absorption, *Opt. Commun.* 197 (2001) 431–437, [https://doi.org/10.1016/S0030-4018\(01\)01406-7](https://doi.org/10.1016/S0030-4018(01)01406-7).
- [61] R. Philip, P. Chantharasupawong, H. Qian, R. Jin, J. Thomas, Evolution of nonlinear optical properties: From gold atomic clusters to plasmonic nanocrystals, *Nano Lett.* 12 (2012) 4661–4667, <https://doi.org/10.1021/nl301988v>.

- [62] G. Krishna Podagatlapalli, S. Hamad, S.P. Tewari, S. Sreedhar, M.D. Prasad, S. Venugopal Rao, Silver nano-entities through ultrafast double ablation in aqueous media for surface enhanced Raman scattering and photonics applications, *J. Appl. Phys* 113 (2013), 073106, <https://doi.org/10.1063/1.4792483>.
- [63] K. Zhang, R.A. Ganeev, K.S. Rao, S.K. Maurya, G.S. Boltaev, P.S. Krishnendu, Z. Yu, W. Yu, Y. Fu, C. Guo, Interaction of pulses of different duration with chemically prepared silver nanoparticles: Analysis of optical nonlinearities, *Am. J. Physiol.* 2019 (2019), 6056528, <https://doi.org/10.1155/2019/6056528>.
- [64] H.I. Elim, J. Yang, J. Lee, J. Mi, W. Ji, H.I. Elim, J. Yang, J. Lee, Observation of saturable and reverse-saturable absorption at longitudinal surface plasmon resonance in gold nanorods Observation of saturable and reverse-saturable absorption at longitudinal surface plasmon resonance in gold nanorods, *Hosp. Pedia* 8 (2006), 083107, <https://doi.org/10.1063/1.2177366>.
- [65] N.A. Saad, M.H. Dar, D.N. Rao, Saturable and reverse saturable absorption of a Cu 2 O – Ag nanoheterostructure, *J. Mater. Sci.* 54 (2019) 188–199, <https://doi.org/10.1007/s10853-018-2811-5>.
- [66] K.L. Kelly, E. Coronado, L.L. Zhao, G.C. Schatz, The optical properties of metal nanoparticles: the influence of size, shape, and dielectric environment, *J. Phys. Chem. B* 107 (2003) 668–677, <https://doi.org/10.1021/jp026731y>.
- [67] Y. Ben-Hai, Z. Dong-Ling, L. Ying-Bin, T. Qing-Bin, Nonlinear optical behaviors in a silver nanoparticle array at different wavelengths, *Chin. Phys. B* 22 (2013), 014212, <https://doi.org/10.1088/1674-1056/22/1/014212>.
- [68] S.A. Angayarkanni, V. Sunny, J. Philip, Effect of nanoparticle size, morphology and concentration on specific heat capacity and thermal conductivity of nanofluids, *J. Nanofluids* 4 (2015) 302–309, <https://doi.org/10.1166/jon.2015.1167>.
- [69] S. Li, X. Zhu, B. Wang, Y. Qiao, W. Liu, H. Yang, N. Liu, M. Chen, H. Lu, Y. Yang, Influence of Ag nanoparticles with different sizes and concentrations embedded in a TiO<sub>2</sub> compact layer on the conversion efficiency of perovskite solar cells, *Nanoscale Res. Lett.* 13 (2018) 210, <https://doi.org/10.1186/s11671-018-2626-y>.
- [70] M. Priyadarshini, G. Vijaya Prakash, Saturation and reverse saturation of nonlinear absorption in laser ablated gold nanoparticles, *Mater. Today. Proc.* (2021), <https://doi.org/10.1016/j.matpr.2021.06.375>.
- [71] K. Wang, H. Long, M. Fu, G. Yang, P. Lu, Size-related third-order optical nonlinearities of Au nanoparticle arrays, *Opt. Express* 18 (2010) 13874–13879, <https://doi.org/10.1364/OE.18.013874>.
- [72] A. Salah, A. Mansour, M.B. Mohamed, I.M. Azzouz, S. Elnaby, Y. Badr, Effects of nanoparticles size and concentration and laser power on nonlinear optical properties of Au and Au–CdSe nanocrystals, *Appl. Surf. Sci.* 353 (2015) 112–117, <https://doi.org/10.1016/j.apsusc.2015.06.060>.
- [73] S.K. Maurya, R.A. Ganeev, A. Rout, C. Guo, Influence of PVP polymer concentration on nonlinear absorption in silver nanoparticles at resonant excitation, *Appl. Phys. A* 126 (2019) 26, <https://doi.org/10.1007/s00339-019-3208-2>.
- [74] M. Sheik-bahae, A.A. Said, E.W. Van Stryland, High-sensitivity, single-beam n(2) measurements, *Opt. Lett.* 14 (1989), <https://doi.org/10.1364/OL.14.000955>.
- [75] S. Kumar, M. Venkatesh, R.A. Ganeev, C. Guo, Study of various material particles by third harmonic generation method based on laser pulse induced plasma, *Opt. Mater.* 98 (2019), 109423, <https://doi.org/10.1016/j.optmat.2019.109423>.
- [76] M. Masnavi, N. Nakajima, K. Horioka, H.P. Araghy, A. Endo, Simulation of particle velocity in a laser-produced tin plasma extreme ultraviolet source, *J. Appl. Phys* 109 (2011) 123306, <https://doi.org/10.1063/1.3601346>.
- [77] M. Oujja, J.G. Izquierdo, L. Bañares, R. de Nalda, M. Castillejo, Observation of middle-sized metal clusters in femtosecond laser ablation plasmas through nonlinear optics, *Phys. Chem. Chem. Phys.* 20 (2018) 16956–16965, <https://doi.org/10.1039/C8CP02825G>.
- [78] F. Théberge, N. Aközbek, W. Liu, A. Becker, S.L. Chin, Tunable ultrashort laser pulses generated through filamentation in gases, *Phys. Rev. Lett.* 97 (2006), 023904, <https://doi.org/10.1103/PhysRevLett.97.023904>.
- [79] R.A. Ganeev, H. Singhal, P.A. Naik, J.A. Chakera, M. Kumar, P.D. Gupta, Fourth-order harmonic generation during parametric four-wave mixing in the filaments in ambient air, *Phys. Rev. A* 82 (2010), 043812, <https://doi.org/10.1103/PhysRevA.82.043812>.
- [80] M. Stafe, C. Negutu, N.N. Puscas, Third harmonic from air breakdown plasma induced by nanosecond laser pulses, *Appl. Phys. B* 124 (2018) 106, <https://doi.org/10.1007/s00340-018-6978-x>.
- [81] N. Aközbek, A. Iwasaki, A. Becker, M. Scalora, S.L. Chin, C.M. Bowden, Third-harmonic generation and self-channeling in air using high-power femtosecond laser pulses, *Phys. Rev. Lett.* 89 (2002), 143901, <https://doi.org/10.1103/PhysRevLett.89.143901>.
- [82] R.A. Ganeev, V.I. Redkorechev, T. Usmanov, Optical harmonics generation in low-temperature laser-produced plasmas, *Opt. Commun.* 135 (1997) 251–256, [https://doi.org/10.1016/S0030-4018\(96\)00633-5](https://doi.org/10.1016/S0030-4018(96)00633-5).
- [83] M. Oujja, A. Benítez-ca, R. De Nalda, M. Castillejo, Harmonic generation by atomic and nanoparticle precursors in a ZnS laser ablation plasma, *Appl. Surf. Sci.* 392 (2017) 572–580, <https://doi.org/10.1016/j.apsusc.2016.09.087>.
- [84] P. Balcou, M.Y. Ivanov, A.L. Huillier, P.B. Corkum, Theory of high-harmonic generation by low-frequency laser fields, *Phys. Rev. A* 49 (1994).
- [85] A.M. Perelomov, V.S. Popov, M.V. Terent'ev, Ionization of atoms in an alternating electric field, *Sov. Phys. JETP* 23 (1966).
- [86] Y.H. Lai, J. Xu, U.B. Szafruga, B.K. Talbert, X. Gong, K. Zhang, H. Fuest, M.F. Kling, C.I. Blaga, P. Agostini, L.F. Dimauro, Experimental investigation of strong-field-ionization theories for laser fields from visible to midinfrared frequencies, *Phys. Rev. A* 063417 (2017) 1–10, <https://doi.org/10.1103/PhysRevA.96.063417>.